High Electrical Conductivity 2D MXene Serves as Additive of Perovskite for Efficient Solar Cells

Zhanglin Guo, Liguo Gao, Zhenhua Xu, Siowhwa Teo, Chu Zhang, Yusuke Kamata, Shuzi Hayase, Tingli Ma*

Zhanglin Guo, Zhenhua Xu, Dr. Siowhwa Teo, Chu Zhang, Yusuke Kamata, Prof. Shuzi Hayase, Prof. Tingli Ma
Graduate School of Life Science and Systems Engineering, Kyushu Institute of Technology, Kitakyushu, Fukuoka, 808-0196, Japan
E-mail: tinglima@life.kyutech.ac.jp
Prof. Liguo Gao,
School of Petroleum and Chemical Engineering, Dalian University of Technology, Panjin Campus, Panjin, 124221, P. R. China

MXene, a newly intriguing family of two-dimensional (2D) materials, have recently attracted considerable attention owing to their excellent properties such as high electrical conductivity and mobility, tunable structure and termination groups. In this work, the $Ti_3C_2T_x$ MXene is incorporated into the perovskite absorber layer for the first time, which aims for efficiency enhancement. Results show that the termination groups of the $Ti_3C_2T_x$ can retard the crystallization rate, thereby increasing the crystal size of $MAPbI_3$. We find that the high electrical conductivity and mobility of MXene can accelerate the charge transfer. After optimizing the key parameters, 12% enhancement in device performance is achieved by 0.03 wt% amount of MXene additive. This work unlocks opportunities for the use of MXene as potential materials in PSCs applications.

1. Introduction

The organic-inorganic halide perovskite solar cells (PSCs) have attracted tremendous attentions due to its high-speed development in photo conversion efficiency (PCE) in the past several years.[1-3] Though the highest certified PCE of 23.2% have been achieved,[4] there is

still a long journey to go to achieve its theoretical efficiency limit of 30~33%.[5] Among the components of the PSCs device, the perovskite layer for light absorption and carrier transfer, is always the central part that determines the device performance.[6-8] While the crystal size is the most important parameter for perovskite film. The larger crystal size promises higher charge carrier transformation efficiency and better performance because of less amount of grain boundaries.[9, 10]

With the aim of enlarging the particle size of perovskite crystals, researchers have proposed various kinds of strategies, such as antisolvent optimizing,[11] post-treatment[12] and additive engineering.[13, 14] Among which the additive engineering is very promising and easy to operate. For instance, Wang et al. added water into the perovskite precursor and they found that the water additive can enhance the crystallization and surface coverage.[15] Gratzel group applied poly(methyl methacrylate) (PMMA) as a template to control the nucleation and crystal growth process, consequently, a high PCE of over 21% was achieved.[16] Han and co-workers used methylammonium acetate and thio-semicarbazide as additives has resulted in a high crystalline quality of the perovskite, leading to enhanced PCE and durability of PSCs.[13] Moreover, except the aforementioned soluble additive, some 2D nanomaterials with unique properties have also been used as additives in recent years. For example, Hagfeldt et al. introduced nitrogen-doped graphene into the perovskite layer and all the photovoltaic parameters were improved.[17] The graphene not only enlarged the grain size, but also passivated the perovskite surface and reduced the charge recombination. More recently, another 2D compound, g-C_3N_4, was doped into the perovskite layer.[18] The g-C_3N_4 dopant improved grain size, reduced the intrinsic defect and more importantly, it increased the film conductivity of the perovskite layer. In addition, other 2D materials such as WS_2,[19] MoS_2[20] and black phosphorus[21] have also been used as an additive or buffer layer to improve the performance of the PSCs. Therefore, the 2D layered nanomaterials, featuring with unique

morphology and excellent properties, are very promising additives for PSCs efficiency improvement.

MXene, a newly emerging class of 2D materials with the general formula of $M_{n+1}X_nT_x$, is obtained by selectively etching the A (Al, Sn etc.) layer of MAX phase by hydrofluoric acid (HF) or in-situ generated HF. $Ti_3C_2T_x$ (T_x represents the termination group), a typical MXene, has many outstanding properties including high electronic conductivity (2.0×10^4 S cm^{-1}), high mobility (1 cm^{2}V^{-1}S^{-1}) and charge carrier density (3.8×10^{22} cm^{-3}).[22] More importantly, $Ti_3C_2T_x$ can be tuned by suitable modification of their surface chemistry, which substantially render controllable and extraordinary properties.[23-25] The aforementioned excellent properties ensure the wide applications of MXenes in supercapacitors, transparent electrodes and ion batteries.[22, 26, 27]

Herein, we used a typical MXene material, $Ti_3C_2T_x$, as an additive into the perovskite absorber layer. We found that the termination groups of $Ti_3C_2T_x$ retard the crystallization rate, increase the crystal size of the perovskite layer, and its excellent electrical properties of MXene favor the charge transfer of PSCs. After optimization, a 12% PCE enhancement of PSCs can be obtained with 0.03 wt% amount of MXene additive.

2. Results and Discussion

As a very typical MAX phase, M (Ti element) layers of Ti_3AlC_2 are interleaved with the A (Al element) layers, with the X (C element) atoms filling the octahedral sites between the former.[28] When Ti_3AlC_2 materials are treated in HF solution, the Al layers can be selectively removed from the interlayers by disconnecting the metallic bonds between Al and Ti, resulting into 2D MXene, as schematically depicted in **Figure S1a**. From the scanning electron microscopy (SEM) images, it can be found that the Ti_3AlC_2 displays an irregular morphology, with the size of several micrometers as shown in **Figure S1b**. Upon HF etching, the morphology altered drastically and very uniform micron-sized multilayers were obtained

(**Figure S1c**). The multilayers present loosely packed accordion-like morphology, and the layers were obviously separated from each other, which is similar to the lamellar graphite.

In order to confirm the phase variation brought by HF etching, the samples were tested by X-ray diffraction (XRD) and the patterns are shown in **Figure 1a**. It can be found that the peaks of Ti_3AlC_2 phase disappear after HF etching. The presence of $Ti_3C_2T_x$ main phase indicates the successful etching of the Al layer.[28] The peaks at 36.0° and 41.6° are attributed to the impurity of TiC, which is used as raw materials for Ti_3AlC_2 synthesis and is difficult to be removed during HF etching. The irradiation peaks at 8.9°, 18.3° and 27.7° correspond to the (002), (006), (008) facet of $Ti_3C_2T_x$, respectively.[29, 30] In order to further confirm the element distribution, X-ray photoelectron spectroscopy (XPS) was conducted for the $Ti_3C_2T_x$ multilayers. From the survey region (**Figure 1b**), the signals belonging to the element of C, Ti, O, F were clearly detected without signals for Al, which indicates fully etching of Al layer in MAX phase, in accordance with the XRD results. In the high-resolution XPS spectrum of the Ti 2p (**Figure 1c**), the components centered at 455.0, 455.7, 457.1 and 460.7 eV are assigned as Ti, Ti^{2+}, Ti^{3+} and $TiO_{2-x}F_x$, respectively. For the C 1s spectrum, the curve can be fitted by four components centered at 282.1, 282.0, 284.6, and 285.6 eV, which are attributed to C-Ti-O, C-Ti, C-C, and C-O, respectively. We also analyzed the O 1s spectrum and results displayed that the peaks can be fitted by two peaks at 530.0 and 531.7 eV for Ti-O and O-H, respectively. The existence of Ti-O, O-H, and Ti-F indicates the termination group, T_x, are O, OH, and F, which is in agreement with the previous reports.[31-34] Therefore, the $Ti_3C_2T_x$ multilayers were successfully obtained by HF etching.

The $Ti_3C_2T_x$ multilayers, similar to other 2D materials, can be exfoliated easily due to weak interlayer van der Waals force.[35, 36] Aiming at getting the smaller size and fewer layers, the $Ti_3C_2T_x$ multilayers were exfoliated in water under the sonication with Ar bubbling to avoid oxidation. Then the sample was centrifuged at the speed of 6000 rpm to remove the un-exfoliated multilayers and the impurity of TiC. SEM image of supernatants is shown in

Figure S2 and comparing with the $Ti_3C_2T_x$ multilayers, the size and the number of layers are greatly reduced after sonication. The nanoflakes with the size of ~200 nm are interconnecting with each other, which is due to the incompletely split of large $Ti_3C_2T_x$ layers during the sonication process. Subsequently, the $Ti_3C_2T_x$ nanoflakes were dispersed in DMF.[37] As shown in **Figure S1d**, $Ti_3C_2T_x$ was separated from each other and the size was also further reduced. This can be attributed to the further sonication in a proper solvent, which promotes the splitting of interconnected nanoflakes into independent nanoflakes. At the same time, the dispersing solution displays the Tyndall effect under the irradiation of laser, implying well-dispersion of $Ti_3C_2T_x$ nanoflakes in DMF solvent.

To apply in PSCs, the $Ti_3C_2T_x$ nanoflakes dispersing in DMF solvent were introduced as the additive into the perovskite layer. **Figure S3** shows the photograph of the perovskite precursor, where the solvent is DMF/DMSO mixed solvents. After introducing the $Ti_3C_2T_x$ into the precursor solution, it can be seen that the color changed from luminous yellow to dark yellow since the $Ti_3C_2T_x$ dispersing in solvents display as a black solution. The n-i-p planar structure of PSCs was fabricated to investigate the effect of $Ti_3C_2T_x$ additive on the device performance. The configuration of the devices is ITO/SnO_2/perovskite: $Ti_3C_2T_x$/Spiro-OMeTAD/Au, as shown in **Figure S3**.

Figure S4 displays the XRD patterns of the perovskite film with a different amount of $Ti_3C_2T_x$ additive relative to the weight of the perovskite precursor, from 0 to 0.1 wt%. All the samples present a cubic perovskite phase with a very weak peak belonging to the PbI_2 phase and the main peak at around 14.1° corresponds to (110) crystal plane of $CH_3NH_3PbI_3$ phase. We enlarged the main peak at around 14.1° and it can be found that the peak was slightly shifted towards lower angle while keeping the positions of the other peaks the same. Therefore, the peak shift is attributed to the stress brought by $Ti_3C_2T_x$ additive, suggesting the perovskite crystals experienced homogenous strain during the growing process.[38] We further improved the amount of additive to 0.25 wt% and the obtained sample (**Figure S5**) displays a

similar XRD profile while the main peak at around 14.1° was shifted to a lower angle, as compared to other samples.

In order to further examine the perovskite film quality either with or without additive, the films were characterized by SEM, as shown in **Figure 2**. All the samples are in uniform morphology with no obvious pin-holes, which promises for high device performance. Comparing with the pristine film, the films with MXene additive show larger crystal size, especially 0.03 wt% $Ti_3C_2T_x$. To accurately measure the crystal size of the perovskite films, the specific crystal size distributions were plotted and the results were shown in **Figure S6**. Clearly, the average grain size of the perovskite was increased from 150 to 358 nm after the introduction of 0.03 wt% amount of additive, comparing with that of the sample without an additive. Moreover, all the perovskite films with $Ti_3C_2T_x$ additive possess a larger grain size than that of the perovskite layer without the additive. Generally, the larger grain size of perovskite means less amount grain boundaries, thereby favoring the carrier transformation through the boundaries. This suggests that the addition of $Ti_3C_2T_x$ additive enable the growth of larger perovskite grain size.

SEM images reveal that $Ti_3C_2T_x$ is non-detectable from the perovskite films at low weight ratio (0.01-0.1 wt%) loading. In order to investigate the location of $Ti_3C_2T_x$ additive, we then increased the amount of the additive to 0.25 wt%, as shown in **Figure S7**. Sheet-like particles were on the surface and the boundary of the perovskite film, respectively. To further confirm their composition, we carried out the energy dispersive X-ray spectroscopy (EDX) measurement for the samples, as shown in **Figure S8**. Several peaks attributed to titanium element are observed through EDX spectrum, which indicates the existence of the titanium element.[39] Through the element mapping analysis, it shows that the titanium element is homogeneously distributed. The slightly low signal of titanium element is due to the usage of very low concentration. Therefore, when a small amount of $Ti_3C_2T_x$ additive was introduced into the perovskite film, the sheet particles only existed in the grain boundary. This may then

induce mechanical stress to the perovskite crystals and result in the shift of the main irradiation peak, which is consistent with the XRD results. Whereas, when a larger amount of $Ti_3C_2T_x$ additive was introduced into the film, the excess additive would be extruded to the surface of the film (**Figure S7**). In our previous research using Spiro-OMeTAD as the additive to modify the perovskite film, the excess additive was also extruded to the surface from the grain boundary.[40]

On the basis of the discussion above, we propose a nucleation and growth route of perovskite film with the $Ti_3C_2T_x$ additive, as shown in **Figure 3**. Firstly, the perovskite precursor with or without additive was spin coated on the SnO_2 surface and ethyl acetate was used as anti-solvent. As depicted in the figure, the $Ti_3C_2T_x$ possesses abundant termination groups of O, OH, and F on its surface. In the research of Hagfeldt et al, they used N-doped graphene as an additive. The basic sites on N-doped graphene could interact with the hydrogen atoms of the $[HC(NH_2)_2]$ (FA), which retards the crystallization process and leads to large perovskite grains.[17] The similar situation was also been reported by Liao et al when they used $g-C_3N_4$ as an additive because protonation occurs at the most basic centers.[18] In our case, the basic fluorine on the surface of $Ti_3C_2T_x$ can make the protonation occur with hydrogen atoms of the MA, thus forming the interaction between fluorine and CH_3NH_3 (MA). Moreover, Wang et al[41] found that when N, N′-bis-[2-(ethanoic acid sodium)]-1,4,5,8-naphthalene diimide modified graphene was used as the interface layer between electron selective layer, N-H···I^- van der Waals interaction formed between the modified graphene and MAI. Therefore, in our case, the OH groups are hypothesized to have interaction with MAI, forming O-H···I^- van der Waals interaction. Due to the interaction between the additive and MAI, during the anti-solvent dripping, the nucleus generates around the additive and the number of the nucleus is suppressed, implies retardation in the nucleation process.[42] While without additive, more nucleus will be generated uniformly on the SnO_2 layer. The additive disperses well in the DMF solvent, thus the perovskite precursor may experience a homogeneous nucleation

process. Finally, the perovskite film was annealed on the hot plate, during which the film was transformed to dense perovskite phase. Since the film with additive generates lesser nuclei, the crystal growth is slower than that of the pristine film. After the transformation process, larger perovskite crystals could be obtained in the presence of $Ti_3C_2T_x$ as an additive. Therefore, using $Ti_3C_2T_x$ as an additive can effectively increase the grain size of perovskite film.

The light absorption ability of different perovskite films deposited on SnO_2/ITO substrates were investigated by UV-vis spectra and the results are presented in **Figure 4a**. All the perovskite films show an absorption onset lying at 800 nm together with a spectrally broad absorption feature in the region. By comparing the absorption curves, the perovskite films with $Ti_3C_2T_x$ additive display an enhancement of light absorption abilities. This phenomenon was attributed to the role of the $Ti_3C_2T_x$ present in the perovskite grain crystals. The particle size of the grains deeply influence the scattering behavior of the incident light and the larger grain size can enhance the light scattering.[43, 44] Therefore, the perovskite film with 0.03 wt% additive incorporation rendered the largest crystal size, hence displayed the highest light absorption ability.

Figure 4b and Table 1 display the performance of the devices with and without additive modification. The devices with 0.01, 0.02 and 0.03 wt% of additives show better PCE than the pristine device. The highest PCE of 17.41% for the 0.03 wt% additive based device was achieved with J_{sc}, V_{oc}, and FF of 22.26 mA/cm^2, 1.03 V, and 0.76, respectively in the reverse scan, while 15.54%, 20.67 mA/cm^2, 1.00 V, and 0.75 for the pristine device. The enhancement of J_{sc} in 0.03 wt% additive incorporated device is in agreement with the incident photon-to-electron conversion efficiency (IPCE), as shown in **Figure S9a**. A photocurrent of 21.60 mA/cm^2 is slightly lower (with the difference of 2.96%) when compared to the Jsc of 22.26 mA/cm^2 obtained from *J-V* characteristics. The possible reason for this discrepancy should be attributed to the lower illumination intensity during the IPCE measurement, where

the recombination process is more prominent because of trap states and space charge effects.[45] In order to check the stability of the additive incorporated device, the steady-state photocurrent and efficiency were measured at the maximum power point of 0.848 V (**Figure S9b**). After continuous irradiation for 180 s, the current density and PCE are stabilized at 20.08 mA/cm^2 and 17.03%, respectively, which is well agreed with PCE obtained from the *J-V* curve. The improvement in Jsc for the 0.03 wt% additive based device should be attributed to the large average crystal size and the reduction of small grains (**Figure S6a** and **d**) between larger grains. While further increasing the amount of the additive leads to decrement in PCE of the devices. The striking reduction lies in FF and V_{oc}, which should be attributed to the perovskite-Spiro interface variation with the increasing amount of the additive. This is because when excess $Ti_3C_2T_x$ additive was added to the perovskite film, they would aggregate on the surface of the film, which might act as the carrier recombination centers.[46]

In order to verify the reproducibility of the high efficiencies for the additive incorporated device, we fabricated more cells and the detailed statistics of the photovoltaic parameters for the devices were presented in **Figure 5** and Table 2. The results clearly show that all the parameters were enhanced when the optimum amount of additive was added into the perovskite film. The improvement in FF is ascribed to the larger grains because less amount of total grain boundaries will facilitate the transport and collecting of the charges.[44] Besides the larger crystal size, the increase in V_{oc} can be ascribed to the surface-passivation of the perovskite by $Ti_3C_2T_x$ nanoflakes, which is helpful for improving the hole selectivity and reducing recombination at the perovskite/Spiro interface.[47]

It has been reported that by reducing the internal resistance of the device, the J_{sc} will be increased because higher conductivity can promote the electron transfer process.[48] Therefore, we used the electrochemical impedance spectrum (EIS) method to characterize the device conductivity, as shown in **Figure 6**. The series resistance (R_s) and the charge transfer resistance (R_{CT}) can be extrapolated with the equivalent circuit model consisting of R_s, R_{CT}

and a parallel capacitor C.[18] As a result, it is obvious that the R_{CT} is also reduced from 7000 to 1800 Ω, which means that the conductivity of the perovskite film is increased. Therefore, the high electrical conductivity and mobility of $Ti_3C_2T_x$ additive are beneficial to reduce the charge transfer resistance and promote the charge transfer, consequently enhance the J_{sc}.

Figure S10a gives the steady-state photoluminescence (PL) spectra of perovskite film with and without $Ti_3C_2T_x$ additive on bare glass substrates. The PL intensity of perovskite film with the additive is obviously weaker than that of the pristine perovskite film, meaning an enhanced charge extraction and suppressed carrier recombination.[18, 49] This might be attributed to the better conductivity after introducing high conductivity additive, which is in accordance with the EIS results. Moreover, in order evaluate the dynamics of charge carrier recombination of the perovskite film in the presence of $Ti_3C_2T_x$ additive, we measured the time-resolved PL (TRPL) spectra of the film with and without the additive, as shown in **Figure S10b**. PL lifetime parameters obtained from a biexponential fitting are listed in the Table inserted in **Figure S10b**. We can find that the PL decay is nearly two times slower for perovskite film containing additive (τ_1=12.35 ns) when comparing with the pristine film (τ_1=6.32 ns). The longer lifetimes can be explained by the reduced non-radiative recombination due to the presence of the additive.[17, 50] The TRPL is fully consistent with that in steady-state PL intensity. Therefore, introducing the high conductivity $Ti_3C_2T_x$ additive can result into superior carrier transport behavior of the perovskite film and better device performance.

We also studied the effect of the additive on the *J-V* hysteresis of the devices and the results with forward and reverse scan directions were shown in **Figure S11**. The pristine device displays a large difference between the PCE of 12.46 % (forward scan) and 15.54 % (reverse scan) with the difference of 19.8 %. According to the literature, when the mesoporous structure was employed, the device possesses greatly reduced hysteresis, therefore, the large difference between the performance of forward and reverse scans should be attributed to the planar PSCs configuration in our research.[51, 52] When the additive was incorporated within

10

the perovskite film, the hysteresis, to some extent, was reduced to PCE of 15.03 % (forward scan) and 17.41 % (reverse san) with the difference of 13.7 %. The main reason here is that the enlarged grains reduce the presence of trap states at the grain boundary, resulting in suppressed carrier recombination.[53] Therefore, $Ti_3C_2T_x$ dispersing in DMF is an effective additive to enhance the performance of the PSCs. Besides the DMF, we also used water and DMSO as the solvent for $Ti_3C_2T_x$ additive and the results are shown and discussed in the supporting information.

3. Conclusion

In summary, we have demonstrated a novel strategy to modify the perovskite layer by introducing a 2D layered $Ti_3C_2T_x$ MXene into the perovskite precursor. The additive can retard the nucleation process of the perovskite, resulting in larger grain size. Moreover, the additive with high conductivity and mobility is highly beneficial to accelerate the electron transfer through the grain boundary. After optimizing key parameters, we found that 0.03 wt% is the optimal amount and DMF is the most proper solvent for MXene additive. Accordingly, the highest PCE is improved from 15.54% to 17.41% and the average PCE is increased from 15.18% to 16.80%. This finding thus opens a new pathway to other kinds of MXene materials that are viable for PSCs application, typically for film modification and interface passivation between the perovskite layer and hole transfer layer.

Supporting Information
Supporting Information is available from the Wiley Online Library or from the author.

Received: ((will be filled in by the editorial staff))
Revised: ((will be filled in by the editorial staff))
Published online: ((will be filled in by the editorial staff))

References

[1]   M. Saliba, *Science* **2018**, *359*, 388.

[2]   M. Saliba, J. P. Correa-Baena, M. Grätzel, A. Hagfeldt, A. Abate, *Angew. Chem. Int. Ed.* **2018,** *57*, 2554.

[3]   Z. Guo, L. Gao, C. Zhang, Z. Xu, T. Ma, *J. Mater. Chem. A* **2018,** *6*, 4572.

[4]   N. J. Jeon, H. Na, E. H. Jung, T.-Y. Yang, Y. G. Lee, G. Kim, H.-W. Shin, S. Il Seok, J. Lee, J. Seo, *Nat. Energy* **2018**, *3*, 682.

[5]   A. a. B. Baloch, M. I. Hossain, N. Tabet, F. H. Alharbi, *J. Phys. Chem. Lett.* **2018,** *9*, 426.

[6]   N. J. Jeon, J. H. Noh, W. S. Yang, Y. C. Kim, S. Ryu, J. Seo, S. I. Seok, *Nature* **2015,** *517*, 476.

[7]   J.-P. Correa-Baena, M. Saliba, T. Buonassisi, M. Grätzel, A. Abate, W. Tress, A. Hagfeldt, *Science* **2017,** *358*, 739.

[8]   N. F. Montcada, M. Méndez, K. T. Cho, M. K. Nazeeruddin, E. Palomares, *Nanoscale* **2018,** *10*, 6155.

[9]   A. Listorti, E. J. Juarez-Perez, C. Frontera, V. Roiati, L. Garcia-Andrade, S. Colella, A. Rizzo, P. Ortiz, I. Mora-Sero, *J. Phys. Chem. Lett.* **2015,** *6*, 1628.

[10]   H. S. Jung, N. G. Park, *Small* **2015,** *11*, 10.

[11]   M. Xiao, F. Huang, W. Huang, Y. Dkhissi, Y. Zhu, J. Etheridge, A. Gray-Weale, U. Bach, Y. B. Cheng, L. Spiccia, *Angew. Chem.* **2014,** *126*, 10056.

[12]   L. Hong, Y. Hu, A. Mei, Y. Sheng, P. Jiang, C. Tian, Y. Rong, H. Han, *Adv. Funct. Mater.* **2017,** *27*, 1703060.

[13]   Y. Wu, F. Xie, H. Chen, X. Yang, H. Su, M. Cai, Z. Zhou, T. Noda, L. Han, *Adv. Mater.* **2017,** *29*, 1701073.

[14]   H. Zheng, L. Zhu, L. Hu, S. Yang, S. Chen, A. Alsaedi, T. Hayat, Y. Huang, X. Pan, S. Dai, *J. Mater. Chem. A* **2018**.

[15] X. Gong, M. Li, X. B. Shi, H. Ma, Z. K. Wang, L. S. Liao, *Adv. Funct. Mater.* **2015,** *25*, 6671.

[16] D. Bi, C. Yi, J. Luo, J.-D. Décoppet, F. Zhang, S. M. Zakeeruddin, X. Li, A. Hagfeldt, M. Grätzel, *Nature Energy* **2016,** *1*, 16142.

[17] M. Hadadian, J. P. Correa-Baena, E. K. Goharshadi, A. Ummadisingu, J. Y. Seo, J. Luo, S. Gholipour, S. M. Zakeeruddin, M. Saliba, A. Abate, *Adv. Mater.* **2016,** *28*, 8681.

[18] L. L. Jiang, Z. K. Wang, M. Li, C. C. Zhang, Q. Q. Ye, K. H. Hu, D. Z. Lu, P. F. Fang, L. S. Liao, *Adv. Funct. Mater.* **2018,** *28*, 1705875.

[19] C. Ma, Y. Shi, W. Hu, M. H. Chiu, Z. Liu, A. Bera, F. Li, H. Wang, L. J. Li, T. Wu, *Adv. Mater.* **2016,** *28*, 3683.

[20] A. Capasso, F. Matteocci, L. Najafi, M. Prato, J. Buha, L. Cinà, V. Pellegrini, A. D. Carlo, F. Bonaccorso, *Adv. Energy Mater.* **2016,** *6*, 1600920.

[21] W. Chen, K. Li, Y. Wang, X. Feng, Z. Liao, Q. Su, X. Lin, Z. He, *J. Phys. Chem. Lett.* **2017,** *8*, 591.

[22] A. D. Dillon, M. J. Ghidiu, A. L. Krick, J. Griggs, S. J. May, Y. Gogotsi, M. W. Barsoum, A. T. Fafarman, *Adv. Funct. Mater.* **2016,** *26*, 4162.

[23] Y. Dall'agnese, M. R. Lukatskaya, K. M. Cook, P.-L. Taberna, Y. Gogotsi, P. Simon, *Electrochem. Commun.* **2014,** *48*, 118.

[24] A. N. Enyashin, A. L. Ivanovskii, *The Journal of Physical Chemistry C* **2013,** *117*, 13637.

[25] Q. Peng, J. Guo, Q. Zhang, J. Xiang, B. Liu, A. Zhou, R. Liu, Y. Tian, *J. Am. Chem. Soc.* **2014,** *136*, 4113.

[26] X. Wang, S. Kajiyama, H. Iinuma, E. Hosono, S. Oro, I. Moriguchi, M. Okubo, A. Yamada, *Nat. Commun.* **2015,** *6*, 6544.

[27] M. Naguib, J. Halim, J. Lu, K. M. Cook, L. Hultman, Y. Gogotsi, M. W. Barsoum, *J. Am. Chem. Soc.* **2013,** *135*, 15966.

[28]   A. Feng, Y. Yu, F. Jiang, Y. Wang, L. Mi, Y. Yu, L. Song, *Ceram. Int.* **2017,** *43*, 6322.

[29]   W. Feng, H. Luo, Y. Wang, S. Zeng, L. Deng, X. Zhou, H. Zhang, S. Peng, *RSC Adv.* **2018,** *8*, 2398.

[30]   X. Zhao, M. Liu, Y. Chen, B. Hou, N. Zhang, B. Chen, N. Yang, K. Chen, J. Li, L. An, *J. Mater. Chem. A* **2015,** *3*, 7870.

[31]   P. Lian, Y. Dong, Z.-S. Wu, S. Zheng, X. Wang, S. Wang, C. Sun, J. Qin, X. Shi, X. Bao, *Nano Energy* **2017,** *40*, 1.

[32]   B. Dai, B. Zhao, X. Xie, T. Su, B. Fan, R. Zhang, R. Yang, *J. Mater. Chem. C* **2018,** *6*, 5690.

[33]   X. Zhu, B. Liu, H. Hou, Z. Huang, K. M. Zeinu, L. Huang, X. Yuan, D. Guo, J. Hu, J. Yang, *Electrochim. Acta* **2017,** *248*, 46.

[34]   M. Naguib, M. Kurtoglu, V. Presser, J. Lu, J. Niu, M. Heon, L. Hultman, Y. Gogotsi, M. W. Barsoum, *Adv. Mater.* **2011,** *23*, 4248.

[35]   D. Er, J. Li, M. Naguib, Y. Gogotsi, V. B. Shenoy, *ACS Appl. Mater. Inter.* **2014,** *6*, 11173.

[36]   G. Li, L. Tan, Y. Zhang, B. Wu, L. Li, *Langmuir* **2017,** *33*, 9000.

[37]   K. Maleski, V. N. Mochalin, Y. Gogotsi, *Chem. Mater.* **2017,** *29*, 1632.

[38]   G. Williamson, W. Hall, *Acta Metall.* **1953,** *1*, 22.

[39]   Y. Jiang, X. Wen, A. Benda, R. Sheng, A. W. Ho-Baillie, S. Huang, F. Huang, Y.-B. Cheng, M. A. Green, *Sol. Energy Mater. Sol. Cells* **2016,** *151*, 102.

[40]   L. Gao, L. Wang, X. Ding, E. Zhao, S. Yang, Y. Zhao, Y. Li, S. Wang, T. Ma, *J. Mater. Chem. A* **2018,** *6*, 4365.

[41]   X. Zhao, L. Tao, H. Li, W. Huang, P. Sun, J. Liu, S. Liu, Q. Sun, Z. Cui, L. Sun, *Nano Lett.* **2018,** *18*, 2442.

[42]   S.-S. Li, C.-H. Chang, Y.-C. Wang, C.-W. Lin, D.-Y. Wang, J.-C. Lin, C.-C. Chen, H.-S. Sheu, H.-C. Chia, W.-R. Wu, *Energy Environ. Sci.* **2016,** *9*, 1282.

[43]   C. Lan, S. Zhao, C. Zhang, W. Liu, S. Hayase, T. Ma, *CrystEngComm* **2016,** *18*, 9243.

[44]   Z. Xiao, Q. Dong, C. Bi, Y. Shao, Y. Yuan, J. Huang, *Adv. Mater.* **2014,** *26*, 6503.

[45]   G. Kapil, T. S. Ripolles, K. Hamada, Y. Ogomi, T. Bessho, T. Kinoshita, J. Chantana, K. Yoshino, Q. Shen, T. Toyoda, *Nano Lett.* **2018,** *18*, 3600.

[46]   Y. Bai, X. Meng, S. Yang, *Adv. Energy Mater.* **2018,** *8*, 1701883.

[47]   N. Tripathi, Y. Shirai, M. Yanagida, A. Karen, K. Miyano, *ACS Appl. Mater. Inter.* **2016,** *8*, 4644.

[48]   J. C. Yu, J. A. Hong, E. D. Jung, D. B. Kim, S.-M. Baek, S. Lee, S. Cho, S. S. Park, K. J. Choi, M. H. Song, *Sci. Rep.* **2018,** *8*, 1070.

[49]   Q. Dong, Z. Wang, K. Zhang, H. Yu, P. Huang, X. Liu, Y. Zhou, N. Chen, B. Song, *Nanoscale* **2016,** *8*, 5552.

[50]   Q. Chen, L. Chen, F. Ye, T. Zhao, F. Tang, A. Rajagopal, Z. Jiang, S. Jiang, A. K.-Y. Jen, Y. Xie, *Nano Lett.* **2017,** *17*, 3231.

[51]   H.-S. Kim, N.-G. Park, *J. Phys. Chem. Lett.* **2014,** *5*, 2927.

[52]   H. Oga, A. Saeki, Y. Ogomi, S. Hayase, S. Seki, *J. Am. Chem. Soc.* **2014,** *136*, 13818.

[53]   D.-Y. Son, J.-W. Lee, Y. J. Choi, I.-H. Jang, S. Lee, P. J. Yoo, H. Shin, N. Ahn, M. Choi, D. Kim, *Nat. Energy* **2016,** *1*, 16081.
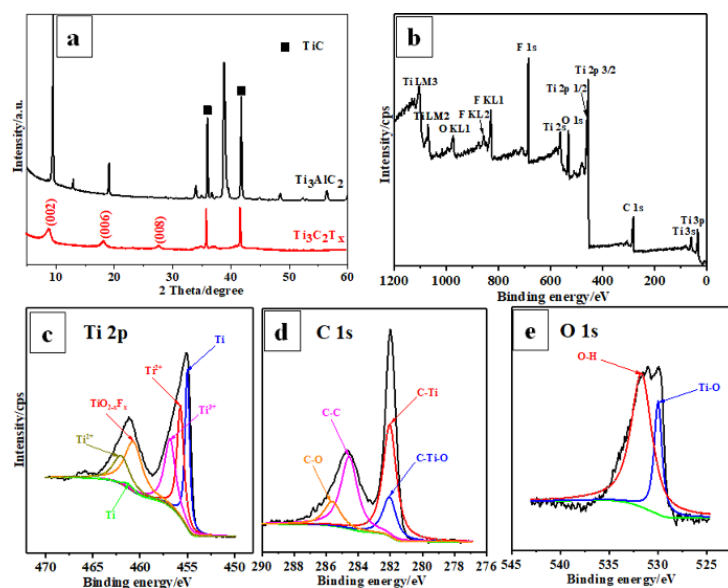
Figure 1. (a) XRD patterns of Ti_3AlC_2 raw materials (black line) and sample after HF etching (red line), (b) XPS spectra of $Ti_3C_2Ti_x$ sample and the high-resolution spectra of (c) Ti 2p, (d) C 1s and (e) O 1s.
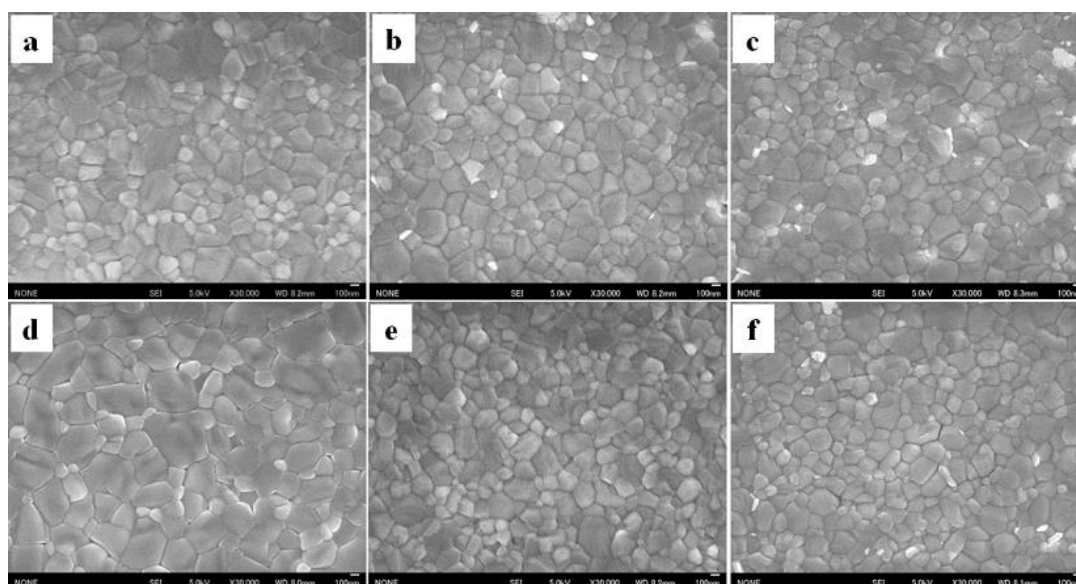

Figure 2. SEM images of the perovskite film with different amount of $Ti_3C_2T_x$-DMF additive: (a) 0 wt%, (b) 0.01 wt%, (c) 0.02 wt%, (d) 0.03 wt%, (e) 0.05 wt% and (f) 0.1 wt%.
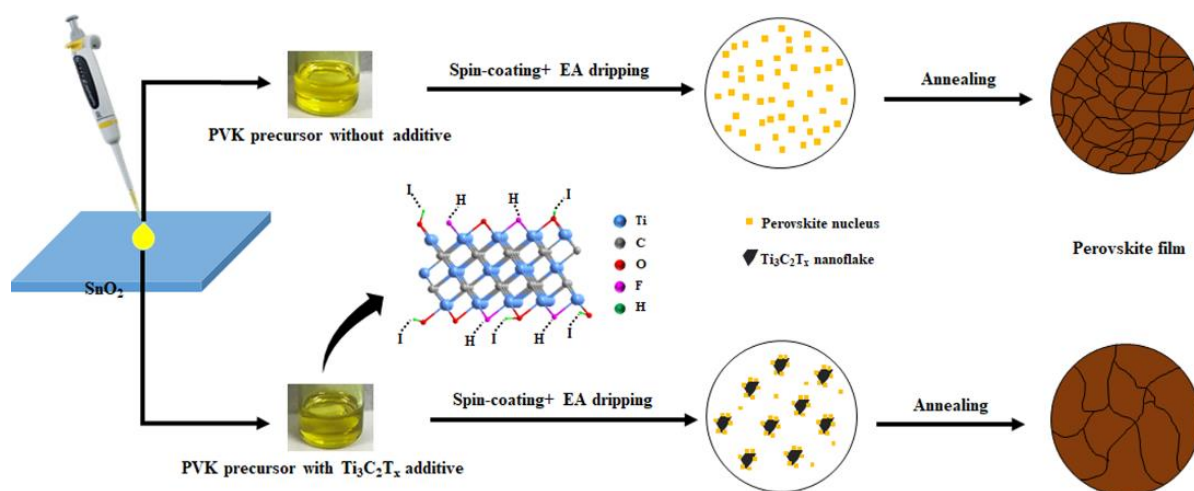
Figure 3. Proposed nucleation and growth route of perovskite film with and without $Ti_3C_2T_x$ additive.

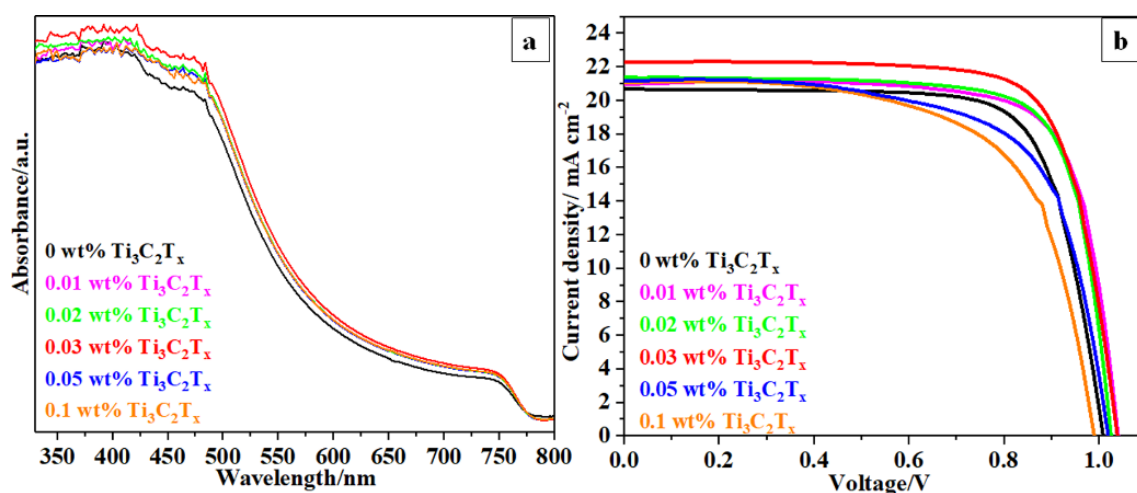**Figure 4.** (a) UV-Vis spectra of the perovskite film and (b) *J-V* curves of PSCs with different amount of $Ti_3C_2T_x$.

Table 1. Performance of PSCs with different amount of $Ti_3C_2T_x$-DMF additive.

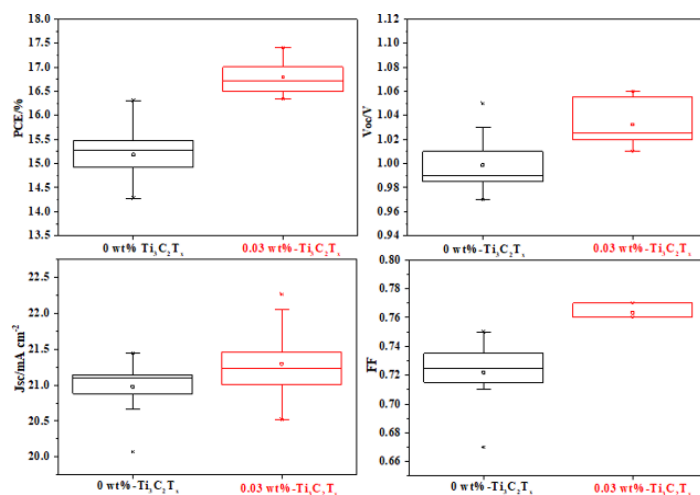| Amount/Parameter	Voc/V	Jsc/mA cm^{-2}	FF	PCE/%
0 wt%	1.00	20.67	0.75	15.54
0.01 wt%	1.03	20.96	0.76	16.54
0.02 wt%	1.02	21.36	0.76	16.68
0.03 wt%	1.03	22.26	0.76	17.41
0.05 wt%	1.01	21.17	0.68	14.49
0.1 wt%	0.98	21.07	0.65	13.49

Figure 5. Photovoltaic statistics for 0 wt% and 0.03 wt% $Ti_3C_2T_x$ additive based device (18 cells for either type): (a) PCE, (b) V_{oc}, (c) J_{sc} and (d) FF.

Table 2. Photovoltaic parameters for 0 wt% and 0.03 wt% $Ti_3C_2T_x$ additive based device (18 cells for either type)

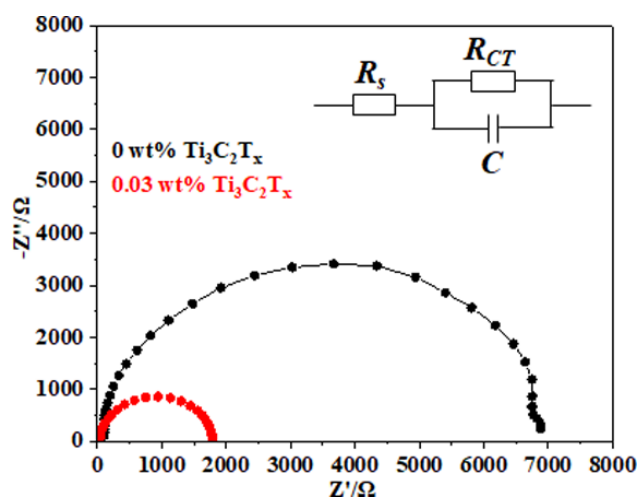| Amount/Parameter	Voc /V	Jsc/mA cm^{-2}	FF	PCE/%
0 wt% $Ti_3C_2T_x$	1.00±0.02	20.98±0.37	0.72±0.02	15.18±0.50
0.03 wt% $Ti_3C_2T_x$	1.03±0.02	21.31±0.51	0.76±0.01	16.80±0.35

Figure 6. (a) Nyquist plots of 0 wt% and 0.03 wt% $Ti_3C_2T_x$ additive based device measured in the dark with a bias of 0.7 V.